AGU PUBLICATIONS

Geophysical Research Letters

RESEARCH LETTER
10.1002/2016GL070775

Key Points:
- GPP scales linearly with SIF from instantaneous to monthly time scales
- Aggregating ecosystem GPP-SIF functions yield a representative landscape relation that matched one obtained directly using tall tower GPP
- GPP-SIF relations showed sensitivity to plant physiology but not spatiotemporal scale

Supporting Information:
- Supporting Information S1

Correspondence to:
J. D. Wood,
woodjd@missouri.edu

Citation:
Wood, J. D., T. J. Griffis, J. M. Baker, C. Frankenberg, M. Verma, and K. Yuen (2017), Multiscale analyses of solar-induced florescence and gross primary production, *Geophys. Res. Lett.*, *44*, 533–541, doi:10.1002/2016GL070775.

Received 8 AUG 2016
Accepted 18 NOV 2016
Accepted article online 22 NOV 2016
Published online 12 JAN 2017

Multiscale analyses of solar-induced florescence and gross primary production

Jeffrey D. Wood[1,2], Timothy J. Griffis[1], John M. Baker[1,3], Christian Frankenberg[4,5], Manish Verma[6], and Karen Yuen[5]

[1]Department of Soil, Water and Climate, University of Minnesota, Twin Cities, Saint Paul, Minnesota, USA, [2]Now at School of Natural Resources, University of Missouri, Columbia, Missouri, USA, [3]Soil and Water Research Unit, USDA-ARS, Saint Paul, Minnesota, USA, [4]Division of Geological and Planetary Sciences, California Institute of Technology, Pasadena, California, USA, [5]Jet Propulsion Laboratory, California Institute of Technology, Pasadena, California, USA, [6]Consulting for Statistics, Computing, and Analytics Research, University of Michigan, Ann Arbor, Michigan, USA

Abstract Solar-induced fluorescence (SIF) has shown great promise for probing spatiotemporal variations in terrestrial gross primary production (GPP), the largest component flux of the global carbon cycle. However, scale mismatches between SIF and ground-based GPP have posed challenges toward fully exploiting these data. We used SIF obtained at high spatial sampling rates and resolution by NASA's Orbiting Carbon Observatory-2 satellite to elucidate GPP-SIF relationships across space and time in the U.S. Corn Belt. Strong linear scaling functions ($R^2 \geq 0.79$) that were consistent across instantaneous to monthly time scales were obtained for corn ecosystems and for a heterogeneous landscape based on tall tower observations. Although the slope of the corn function was ~56% higher than for the landscape, SIF was similar for corn (C_4) and soybean (C_3). Taken together, there is strong observational evidence showing robust linear GPP-SIF scaling that is sensitive to plant physiology but insensitive to the spatial or temporal scale.

1. Introduction

Terrestrial gross primary production (GPP) is the largest global carbon (C) flux [*Beer et al.,* 2010]. Accurately representing GPP in coupled carbon-climate models is thus of great importance, but a lack of observational constraints at regional to global scales has impeded the development and evaluation of models [*Friedlingstein*, 2015]. Therefore, obtaining better constraints on spatiotemporal variations in GPP is a subject of great interest [*Anav et al.,* 2015]. The advent of satellite-based monitoring of solar-induced fluorescence (SIF) has opened new avenues for probing regional-to-global photosynthesis [*Frankenberg et al.,* 2011b; *Joiner et al.,* 2011, 2014; *Guanter et al.,* 2014; *Porcar-Castell et al.,* 2014; *Duveiller and Cescatti*, 2016]. An important advantage of SIF is that it is more tightly coupled to physiological processes than vegetation indices such as the normalized difference vegetation index (NDVI) [*Rossini et al.,* 2015] or enhanced vegetation index (EVI) that are not sensitive to dynamic changes in physiological functioning and light-use efficiencies (LUEs). For instance, the onset and shutdown of photosynthesis, which is not mechanistically linked to leaf greenness, is better constrained by SIF [*Joiner et al.,* 2014]. However, to fully exploit the potential of SIF, a better understanding of the relationship between SIF and GPP is needed to construct seasonal and annual budgets. This is particularly important for agroecosystems where despite a similar coupling between the electron transport rate (ETR) and fluorescence, different electron-use efficiencies (EUEs) and carbon-use efficiencies (CUEs) can give rise to different SIF-GPP relationship in C_3 and C_4 crops [*Y. Zhang et al.*, 2014]. In the Corn Belt, which is dominated by corn (C_4) and soybeans (C_3), the GPP of the latter is only ~55% of the former [*Suyker and Verma*, 2012]. Understanding how C_4 and C_3 photosynthesis affects the relationship between SIF and GPP is thus important for utilizing SIF toward reliable estimation of local and regional budgets of photosynthetic carbon assimilation.

The existence of a relationship between fluorescence and the ETR of photosystem II is well established at molecular to leaf levels over short time scales, largely based on active fluorimetry measurements [*Baker*, 2008]. In contrast, remote sensing measures passive fluorescence induced by solar irradiance, with significant knowledge gaps regarding quantitative relations with photosynthesis [*Porcar-Castell et al.,* 2014]. Empirically, model and flux tower GPP scales linearly with SIF observed (e.g., Global Ozone Monitoring Experiment 2, (GOME-2) or Greenhouse Gases Observing Satellite (GOSAT)) at coarse spatial resolution and biweekly to annual time scales [*Frankenberg et al.,* 2011b] in a fashion that is somewhat ecosystem

specific [*Guanter et al.,* 2012, 2014; *Parazoo et al.,* 2014]. Asymptotic relationships consistent with light saturation have also been observed between instantaneous SIF and GPP in managed and unmanaged ecosystems based on airborne measurements [*Damm et al.,* 2015]. There is therefore a pressing need to better understand how SIF is linked with GPP across a range of spatiotemporal scales to fully exploit these new observations in a GPP mapping context [*Porcar-Castell et al.,* 2014; *Yang et al.,* 2015].

The Orbiting Carbon Observatory-2 (OCO-2) satellite provides new capacity for space-based monitoring of SIF, with high spectral resolution and signal-to-noise ratios, as well as small footprints (1.3 × 2.3 km) within an orbital track [*Frankenberg et al.,* 2014]. These new monitoring capabilities allow for more detailed assessments of within orbital track spatial gradients in SIF. Furthermore, they permit better matching between satellite and ground-based observations for elucidating the relationships between SIF and GPP compared to previous products [*Frankenberg et al.,* 2011b; *Guanter et al.,* 2014; *Joiner et al.,* 2014; *Parazoo et al.,* 2014] that were to a certain extent hindered by low spatial resolution (10 km diameter for GOSAT and 40 × 80 km for GOME-2) and sampling rates (GOSAT) because of the need for substantial aggregation in space, time, or both. The new high resolution and amount of OCO-2 observations offer the potential for using SIF for finer-scale assessments of GPP-SIF relationships when retrievals are proximal to ground-based flux towers.

The objectives of this current work are to therefore use OCO-2 observations to (i) compare SIF with common VIs, (ii) examine GPP-SIF relations based solely on satellite-based SIF and ground-based GPP observations across instantaneous to monthly time scales and ecosystem (tens to hundreds of meters) to landscape (thousands to ten thousands of meters) scales, and (iii) evaluate regional (hundreds to thousands of kilometers) GPP estimated using the empirical GPP-SIF scaling function approach for a domain encompassing Iowa and southern Minnesota.

2. Materials and Methods

This analysis was conducted using data collected during the year 2015.

2.1. Tower-Based GPP Observations

GPP was inferred [*Reichstein et al.,* 2005; *Moffat et al.,* 2007] in a conventional corn field (AmeriFlux US-Ro1) [*Baker and Griffis*, 2005; *Griffis et al.,* 2005, 2008] and a restored prairie (AmeriFlux US-Ro4), and at the landscape scale at a very tall tower (KCMP 89.3 FM) [*Griffis et al.,* 2010; *X. Zhang et al.,* 2014], both of which are located ~25 km south of the Minneapolis-Saint Paul metropolitan area. GPP was obtained by gap filling and partitioning the net fluxes that were measured using eddy covariance at half-hourly and hourly resolution for ecosystem and tall tower sites [*Yi et al.,* 2000; *Davis et al.,* 2003], respectively. The corn observations, for which flux footprints [*Kljun et al.,* 2004] were typically characterized by 90% isopleths of 60–100 m, were made in a relatively flat 17 ha field, with 180 m of fetch in all directions [*Griffis et al.,* 2007]. At the tall tower (44.689256°, −93.072817°; 290 m above sea level), the fluxes measured at 185 m (above ground level) had typical 90% flux isopleths on the order of 3–5 km that encompassed mixed land cover representative of the surrounding region [*Griffis et al.,* 2010; *X. Zhang et al.,* 2014]. A more detailed description of tower-based flux measurements is provided in the supporting information.

2.2. Satellite Observations

The OCO-2 spectrometer measures spectra in the O_2-A band (757–775 nm, full width at half maximum = 0.042 nm), with far-red SIF retrieved at 757 (F_{757}) and 771 (F_{771}) nm based on the infilling of Fraunhofer lines [*Frankenberg et al.,* 2011a, 2014]. The spatial resolution is 1.3 × 2.3 km, with an eight-footprint along-track sample giving a swath width of 10.6 km, with a 32 day repeat cycle for nadir retrievals. We used the SIF Lite product (v. B7101r), where biases were corrected using observations from reference target areas on a daily basis, similar to methods employed for GOSAT SIF retrievals [*Frankenberg et al.,* 2011b]. When evaluating GPP-SIF relationships at daily to monthly time scales, we applied the daily correction factor that is provided in the SIF Lite product to convert instantaneous observations, F_s, to a 24 h mean, $\overline{F_s}$ [*Frankenberg et al.,* 2011b], with biweekly and monthly $\overline{F_s}$ computed from the interpolated annual cycle (Figure S1). When relations with VIs were examined, F_s was ratioed by the cosine of the solar zenith angle.

We used normalized difference vegetation index (NDVI) and enhanced vegetation index (EVI) Moderate Resolution Imaging Spectroradiometer (MODIS) products (MYD13Q1 v5) from the Aqua satellite, which

provides global coverage every 16 days at 250 m resolution. The fraction of photosynthetically active radiation (PAR) absorbed by the canopy (FPAR) was obtained from the combined MODIS product (MCD15A2, v5) that provides global coverage every 8 days at 1 km resolution. We used the MODIS GPP product (MYD17A2H, v6), which follows an LUE approach and provides global coverage every 8 days at 500 m resolution [*Zhao et al.,* 2005]. Land cover data were obtained from the U.S. Department of Agriculture's National Agricultural Statistical Service National Cropland Data Layer (NCDL) (https://nassgeodata.gmu.edu/CropScape/). An important feature of the NCDL is that it partitions croplands into different types (i.e., >50) and is of very high (30 m) spatial resolution allowing for fine-scale variations of crop distributions within OCO-2 footprints to be estimated. For each SIF retrieval, the fractional corn, soybean, alfalfa, fallow, grassland, forest, wetland, forest, and urban land cover was determined. We also mapped each SIF retrieval to the aforementioned MODIS data.

2.3. GPP-SIF Relationships

Corn-specific and landscape-scale GPP-SIF relationships were obtained using GPP inferred at the field scale and from the tall tower, respectively, and OCO-2 SIF. Prior to establishing GPP-SIF scaling functions, retrievals were screened based on several criteria to ensure representativeness of the relationships for a broader region. For establishing GPP-SIF relationships, retrievals from within 125 km of the tall tower and from directions between 110° and 270° were selected for calibrating the landscape-scale function. Land cover within this defined area was known to be representative of the larger Corn Belt region [*Griffis et al.,* 2010; *X. Zhang et al.,* 2014]. This was confirmed here by a comparison, which found similar land cover distributions for OCO-2 footprints in this calibration domain versus those for all of Iowa and southern Minnesota. When selecting retrievals for establishing the corn-scaling function, only those with >70% corn land cover were used; therefore, the distance from the tower was relaxed to 225 km to increase the number of available observations.

2.4. Regional GPP Analysis

An analysis was performed to examine the validity of using the landscape GPP-SIF scaling function (described in section 2.3) in conjunction with gridded SIF for estimating GPP for a region comprising Iowa and southern Minnesota. Data were gridded at 0.5° resolution over a domain spanning 40.5 to 45°N latitudes and 90 to 96.5°W longitudes. Two data sets were gridded: (i) GPP from SIF (GPP_{SIF}) and (ii) GPP from MODIS (GPP_{MOD}). The GPP_{SIF} was obtained by gridding and interpolating $\overline{F_s}$ for each month and then applying the landscape-scale function. The calibration domain (described in section 2.3) that was used to establish the landscape GPP-SIF function represented a small percentage (<5%) of the larger region of interest.

3. Results and Discussion

3.1. SIF and VIs

We first examined F_s-VI and F_s-land cover relations for retrievals in Iowa and southern Minnesota. At the OCO-2 footprint level, F_s was correlated with EVI ($r = 0.69$), NDVI ($r = 0.69$), and FPAR ($r = 0.70$) from 15 April to 15 October. All F_s-VI joint distributions displayed regions of highest density when F_s was near 0 (Figures 1a–1c); however, the near-binary nature of phenology, which transitions rapidly from barren fields to oases and then senesced crops, is particularly evident in the F_s-NDVI (Figure 1b) and F_s-FPAR (Figure 1c) relations. Both FPAR and NDVI displayed clouds of high data density at the upper and lower ranges, with sparse data coverage in between. Interestingly, the clustering at NDVI > 0.8 showed signs of saturation, as indicated by an apparent change in slope in the higher point cloud. In contrast, the F_s-EVI distribution was consistent across an EVI range of 0.4–0.7, with no apparent signs of saturation. Indeed, NDVI and EVI displayed a nonlinear relationship indicative of saturation of the former ($NDVI = 1.79 \times EVI/[EVI + 0.72]$; $R^2 = 0.97$; Figure S2).

At the height of the growing season, F_s increased with fractional land cover for corn and soybean (Figures 1d and 1e, respectively). Linear correlations were, however, weaker than with the VIs for both corn ($r = 0.25$, $p < 0.001$) and soybean ($r = 0.19$, $p < 0.001$). This was likely because low corn and soybean cover does not imply that the remainders of the footprints were occupied by nonfluorescing surfaces. A stronger relation between F_s and combined corn-soybean land cover emerged ($r = 0.32$, $p < 0.001$), although the majority of data were clustered in a high-density cloud above 0.8 (Figure 1f). Linear fits of F_s on fractional crop cover

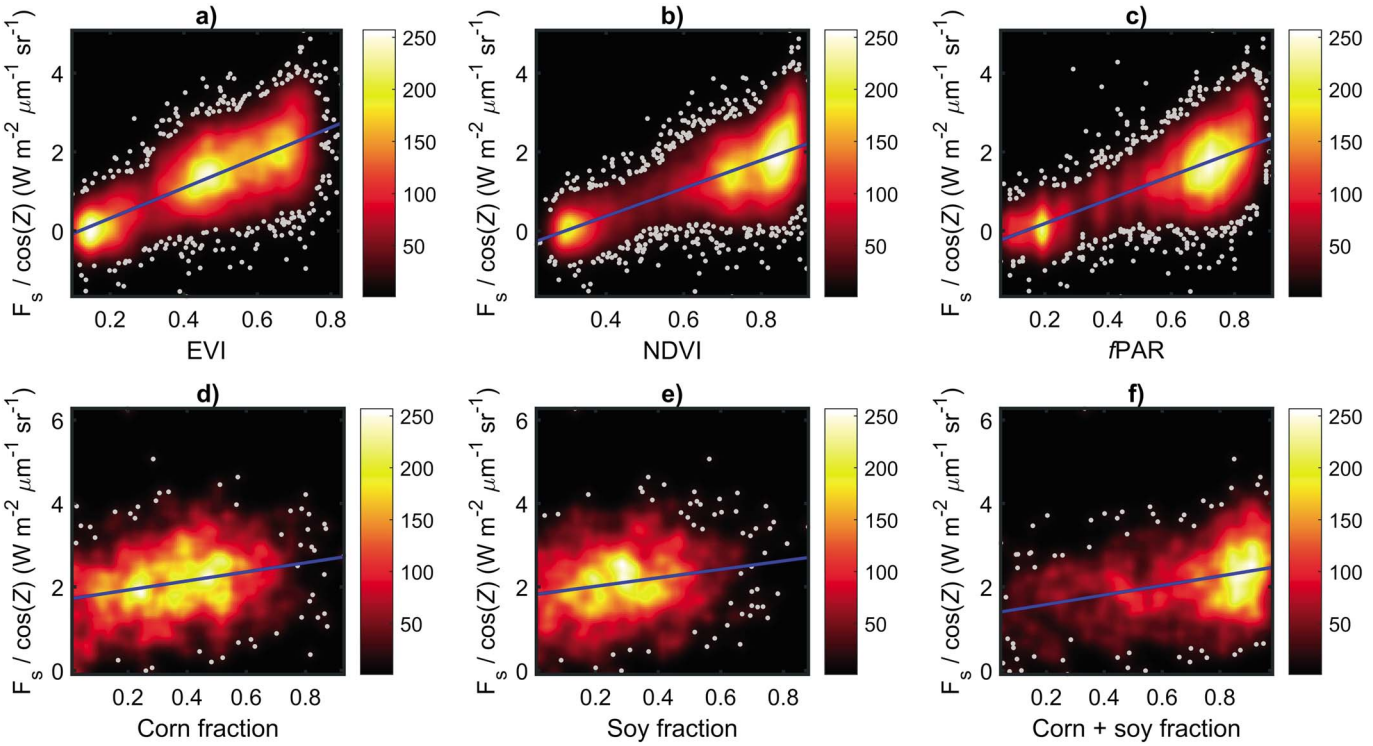

Figure 1. Joint distribution and linear fits of instantaneous SIF (F_s) at 757 nm normalized by the cosine of the solar zenith angle (Z) from April to October 2015 and (a) EVI, (b) NDVI, (c) FPAR, and the fraction of the SIF footprint covered by (d) corn and (e) soybean and (f) the sum of corn and soybean. The color map represents the observation density, and gray points denote observations where the smoothed density is <10% of the maximum density.

had slopes that were not statistically different ($p > 0.1$) between corn (1.09 ± 0.130, $p < 0.001$), soybean (1.01 ± 0.154, $p < 0.001$), and corn + soybean (1.13 ± 0.100), providing empirical evidence for similar fluorescence from corn and soybean canopies.

We also examined F_s-absorbed photosynthetically active radiation (APAR) joint distributions. This analysis was restricted to retrievals within the calibration domain (section 2.3) because the downwelling PAR observations were from a single point. Further filtering was performed to include only cases where leaf area index (LAI) exceeded 25% of the mean domain-wide maximum LAI. The joint F_s-APAR densities from May to October revealed a weak linear relation (Figure S3) that explained 36% of the total variance, with no apparent sign of saturation.

A novel aspect of this present work is that analyses of SIF-VI relations were conducted without aggregating data in space or time, which has been common with earlier SIF products from GOSAT [*Frankenberg et al.,* 2011b] or GOME-2 [*Joiner et al.,* 2013; *Guanter et al.,* 2014] due to the high noise in a single SIF sounding and the coarse spatial resolution. This averaging could potentially introduce artifacts in subsequent analyses through altering the data distribution. Although there is considerable noise in a single OCO-2 retrieval (0.3–0.5 $W\,m^{-2}\,\mu m^{-1}\,sr^{-1}$), the ensemble average of multiple retrievals can be accurate to within 0.05 $W\,m^{-2}\,\mu m^{-1}\,sr^{-1}$ [*Frankenberg et al.,* 2014], with calibration strategies similar to GOSAT [*Frankenberg et al.,* 2011b] being employed for space-based OCO-2 observations, using nonfluorescing reference targets on a daily basis. In analyzing SIF-VI relations at the footprint level, random errors due to the noisy retrievals contribute to scatter; however, the functional relation is expected to be accurate and free of potential distortion due to averaging over space or time.

The F_s-NDVI ($r = 0.69$) and F_s-FPAR ($r = 0.69$) correlations were in line with previous reports for an ensemble of biomes ($r = 0.68$) [*Frankenberg et al.,* 2011b]. The bimodal joint densities (for NDVI and FPAR) were consistent with the fact that most crops in the region have traits selected to maximize light interception to confer rapid growth and probably behaved as influential "points." Our land cover analyses that took advantage of the high spatial resolution of both OCO-2 and the NCDL provided direct empirical evidence that supports

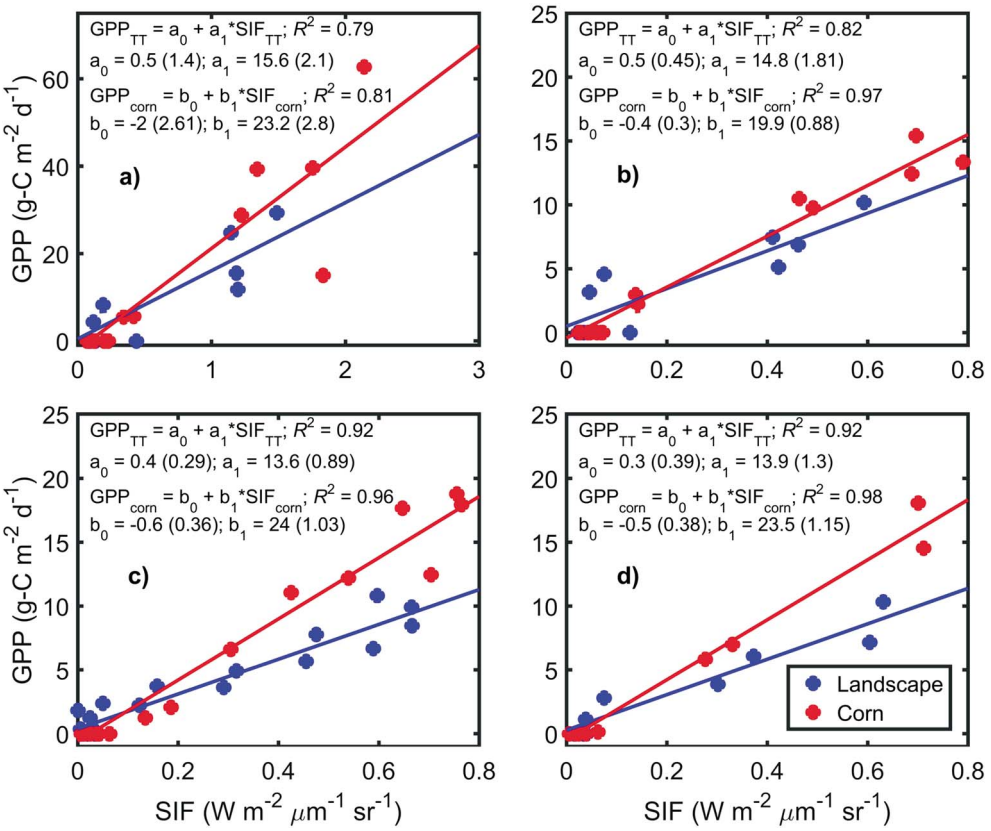

Figure 2. Linear relationships between GPP and SIF in the vicinity of the flux towers were consistent across time scales ranging from (a) instantaneous measurements at the time of the OCO-2 overflight, (b) daily means, (c) biweekly means, and (d) monthly means. In equations, values in parentheses represent standard errors; no intercepts were significant ($p > 0.1$), and all slopes were significant ($p < 0.001$).

the notion that canopy fluorescence is similar for corn and soybean (Figures 1e–1f) [*Y. Zhang et al.,* 2014; *Guan et al.,* 2015]. It is noteworthy that the F_S-APAR joint densities displayed a linear relation, which is encouraging from the perspective of validating the empirical scaling approach for GPP estimation [*Porcar-Castell et al.,* 2014]. The cloud of high data density spanning middle to upper range APAR (175–275 W m^{-2}) may partially explain the relatively low R^2 of 0.36. While EVI clearly has higher sensitivity and less susceptibility to saturation compared to NVDI, as expected [*Huete et al.,* 2002], the question remains as to whether SIF offers advantages in terms of capturing the on-off nature of photosynthesis that gives rise to an intense seasonal cycle of net CO_2 exchange in the region [*X. Zhang et al.,* 2014].

3.2. GPP-SIF Relationships

Strong linear GPP-SIF relationships were obtained for corn ($R^2 \geq 0.81$) and for the mixed landscape ($R^2 \geq 0.79$) for time scales spanning from instantaneous to monthly means (Figure 2). The slopes were significantly higher ($p < 0.001$) for corn versus the landscape for all time scales examined. It is noteworthy that there was consistency in the slopes for both corn and the landscape functions across time scales. Note that unless otherwise stated, the slopes of scaling functions are reported in units of g C m^{-2} d^{-1} (W m^{-2} μm^{-1} sr^{-1})$^{-1}$. Although the goodness of fit was poorer for the instantaneous fits (Figure 2a) versus the daily, biweekly, and monthly means (Figures 2b–2d), consistency in the slope terms demonstrates the existence of robust GPP-SIF relationships that are consistent across time scales.

The scaling functions obtained here were parameterized using GPP and SIF observations with substantially improved scale matching, particularly for the landscape case, compared to earlier works [*Frankenberg et al.,* 2011b; *Guanter et al.,* 2014; *Parazoo et al.,* 2014], for which averaging over expansive space (2° × 2° or coarser), long times (annual or longer), or both was required. Previously reported scaling functions [*Frankenberg et al.,* 2011b; *Parazoo et al.,* 2014] derived from GPP from the Max Planck Institute for

Biogeochemistry (MPI-BGC) [*Beer et al.,* 2010; *Jung et al.,* 2011] model and SIF from GOSAT (for which fluorescence is retrieved at similar wavelengths to OCO-2) [*Frankenberg et al.,* 2011a] are in broad agreement with those found in this present work. The slope of the corn functions was higher than for the croplands (17.1 ± 0.83) in *Parazoo et al.* [2014] that represented a mixture of C_3 and C_4 species. The slopes of the landscape GPP-SIF relationships (13.6–15.6) were considerably lower than the corn-specific case, which is consistent with the presence of plant species that have lower CUE [*Y. Zhang et al.,* 2014; *Guan et al.,* 2015], since measured fluorescence is an integrated metric representative of subfootprint heterogeneity [*Frankenberg et al.,* 2014]. While this finding is consistent with biophysical and measurement theory, it has not been reported previously, where estimates of ensemble across-biome GPP-SIF relationships converged to a value of 18–20 $g\,C\,m^{-2}\,d^{-1}$ $(W\,m^{-2}\,\mu m^{-1}\,sr^{-1})^{-1}$ [*Frankenberg et al.,* 2011b; *Parazoo et al.,* 2014], exceeding the ecosystem-specific scaling functions in *Parazoo et al.* [2014] by 5–185%. This discrepancy may have been due to aggregating to coarse grids and annual means or biases introduced by the distribution of the pooled data.

The linearity of the instantaneous GPP-SIF relations (Figure 2a) indicates the absence of light saturation effects, which is consistent with analyses using SIF products from GOME-2 [*Guanter et al.,* 2014] and GOSAT [*Frankenberg et al.,* 2011b; *Guanter et al.,* 2012; *Parazoo et al.,* 2014]. Previous satellite-based SIF products did not permit the examination of GPP-SIF relationships at subannual time scales because substantial spatiotemporal aggregation of SIF retrievals was required. It is therefore possible that the linear relations in these cases were an artifact of averaging over space and time. Asymptotic instantaneous GPP-SIF relations have been found by others using airborne SIF for multiple ecosystem types [*Damm et al.,* 2015], although linearization of the light response tends to occur when moving from leaf to canopy scale and with increasing spatiotemporal aggregation [*Ruimy et al.,* 1995]. For the first time, we demonstrated that the GPP-SIF relationship was consistent across instantaneous to monthly time scales for both corn and landscape functions (Figure 2). It is therefore unlikely that the linear scaling was related to temporal aggregation.

The landscape investigated here was dominated by corn, soybean, and grasslands, for which the light response [*Gilmanov et al.,* 2010] is generally less prone to saturation compared to forests [*Griffis et al.,* 2003]. Indeed, ecosystem-scale GPP light responses displayed low levels of saturation when considering half-hourly ("instantaneous") data, with further linearization with increasing temporal (Figures S4a–S4c) or spatial (Figure S4) aggregation. While saturation in the GPP light response was relatively muted (Figure S4), the instantaneous GPP-SIF relationship (Figure 2a) showed no evidence of nonlinearity. Our analysis of instantaneous observations was limited to the time of OCO-2 overpasses (13:30 local time); thus, it is possible that the absence of data at other times of day acted to linearize the GPP-SIF relation.

Recent evidence based on ground-based eddy covariance and spectrometer systems supports that light saturation may induce nonlinearity in the GPP-SIF relationship. In a deciduous broadleaf forest, the slope of the GPP-SIF relationship parameterized using instantaneous observations was steeper in the morning (09:30) versus the afternoon (13:30), implying saturation effects under conditions of high light [*Yang et al.,* 2015]. They also noted that the instantaneous afternoon relation (versus the morning case) was in considerably better agreement with the linear one established based on daily means. In contrast, linear GPP-SIF scaling was found for ensembles of half-hourly means for all times of day in corn and wheat fields [*Liu et al.,* 2017]. Collectively, these observations are consistent with the notion that croplands tend to display a more linear light response compared to forests where saturation is common at high incident solar radiation [*Ruimy et al.,* 1995].

The assumption of a linear GPP-SIF relation is critical to the empirical scaling approach for GPP estimation [*Guanter et al.,* 2014; *Parazoo et al.,* 2014; *Porcar-Castell et al.,* 2014]. The consistency in the landscape relationship across time scales observed here provides strong evidence supporting the existence of such linear scaling. As an additional assessment of the robustness of GPP-SIF functions, we compared landscape relations obtained using bottom-up and top-down approaches. The bottom-up function was taken as the sum of ecosystem-specific relations weighted by land cover. The top-down function obtained directly from tall tower measurements was integrated over several ecosystem types for which we did not have direct observational constraints. Given that corn and soybean canopies fluoresce at similar rates as discussed previously, a soybean-specific function was estimated by multiplying our biweekly corn relationship by a factor of 0.55, which is the approximate soybean:corn GPP ratio [*Suyker and Verma*, 2012], while the scaling functions of *Parazoo et al.* [2014] were used for deciduous forests, grasslands, and other croplands. The bottom-up

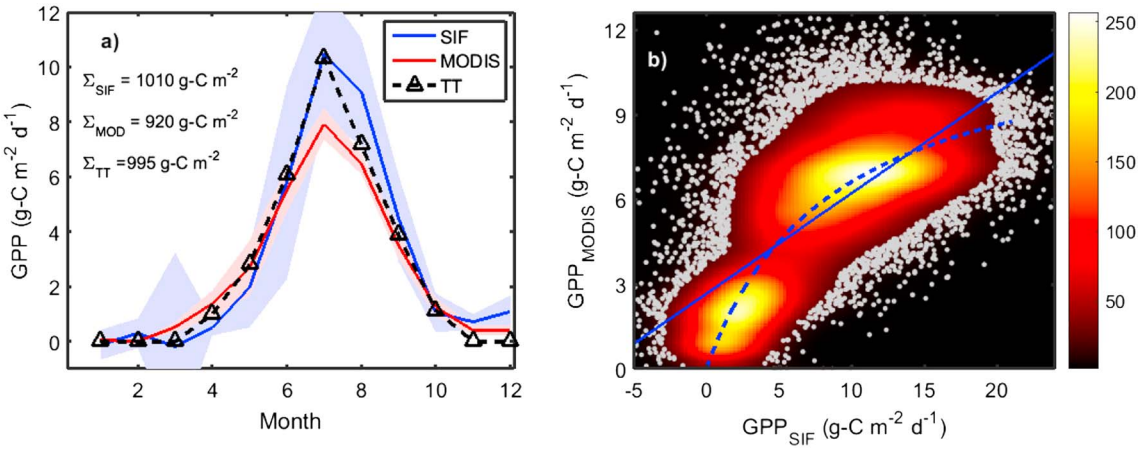

Figure 3. (a) Mean GPP estimated by applying the landscape relationship to gridded and interpolated SIF (GPP_{SIF}), the MODIS product (GPP_{MOD}), and the tall tower (GPP_{TT}), where shading represents 1 SD and (b) the joint distribution of GPP_{MOD} and GPP_{SIF} applied at the footprint level where the solid and dashed lines are linear ($GPP_{MOD} = 0.36 \times GPP_{SIF} + 2.7$; $R^2 = 0.54$) and nonlinear ($GPP_{MOD} = 12.4 \times GPP_{SIF}/[GPP_{SIF} + 8.7]$; $R^2 = 0.65$) fits. In Figure 3b the color map represents observation density, and gray points denote observations where the smoothed density is <10% of the maximum density.

relation (14.5 g C m^{-2} d^{-1} (W m^{-2} μm^{-1} sr^{-1})$^{-1}$) agreed to within 6% of that derived from the tall tower top-down approach using biweekly means (13.6 g C m^{-2} d^{-1} (W m^{-2} μm^{-1} sr^{-1})$^{-1}$) (Figure S5). The excellent agreement provides further evidence for robust linear scaling relations and supports the conclusion that SIF integrates over subgrid heterogeneity unlike reflectance-based products [*Frankenberg et al.,* 2014].

Our analyses of GPP-SIF relationships (Figure 2) and light responses (Figure S4) that are based solely on observations clearly demonstrate robust scaling functions that are independent of temporal aggregation. These types of analyses have not been possible previously due to limitations of previous SIF products, which required severe spatiotemporal averaging (e.g., annual or longer) and in many cases relied on comparison with model GPP. Ecosystem-scale studies have shown that at subdaily time scales, GPP-SIF relations do not saturate in agricultural systems [*Liu et al.,* 2017] or that in ecosystems such as forests that may display saturation, there is good agreement between linear GPP-SIF functions parameterized using daily means or instantaneous observations at 13:30 local time [*Yang et al.,* 2015]. Taken together, there is compelling evidence supporting that linear GPP-SIF scaling relationships are consistent across space and time and contain ample information for regional- to global-scale GPP mapping applications based on remotely sensed SIF. Further studies that link fluorescence from leaf to canopy scales are urgently needed to permit the prying of more mechanistic information out of the remotely sensed SIF signal.

3.3. Regional Analyses

The ensemble, domain-wide means of gridded annual GPP for Iowa and southern Minnesota from SIF (GPP_{SIF}) and MODIS (GPP_{MOD}) were 1010 ± 125 g C m^{-2} (±SD) and 920 ± 100 g C m^{-2}, respectively. However, GPP_{MOD} followed a normal distribution ($p = 0.25$) while GPP_{SIF} did not ($p < 0.01$), displaying negative skewness (−0.55). There was a systematic underestimation by GPP_{MOD} compared to GPP_{SIF} and GPP_{TT} during July and August, with the SIF-based approach capturing the growing season peak (Figure 3a). In contrast, the MODIS-based approach showed susceptibility to saturation. Indeed, at the OCO-2 footprint level, an asymptotic relationship between GPP_{MOD} and GPP_{SIF} was observed ($R^2 = 0.65$), indicating saturation of the former (Figure 3b). The relation is shown in GPP_{MOD}-SIF space in Figure S6.

The empirical scaling approach offers a reasonably direct method of accessing regional to global GPP using satellite-based SIF observations and land cover data—without the need for additional information on vegetation characteristics and gridded meteorological fields. At this juncture, it appears as though land cover classification and the application of ecosystem-specific relationships are needed for operational GPP estimation. Similar analyses of GPP-SIF relationships should be performed using OCO-2 observations and flux towers situated in ecosystems not considered here to better constrain the diversity of scaling functions to determine whether a simplified classification is acceptable. While the calibration of landscape-scale functions and application to a broader region is a potential alternative to obviate the need for fine-scale land use

classification, landscape relationships are likely subject to greater interannual variations in response to changes in land cover than for individual ecosystems.

4. Conclusions

We have made use of OCO-2 SIF observations obtained at high spatial sampling rates and resolution in combination with ecosystem to landscape-scale flux observations to further our understanding of GPP-SIF relationships. It is noteworthy that these analyses were possible in a single growing season because of the high SIF sampling rates (along orbital tracks) and spatial resolution, and thus relatively free of artifacts introduced by scale mismatches in space and time. For instance, we did not have to average croplands over multiple years to ensure that the flux tower and SIF signals represented the average of crop rotations, and all satellite and flux tower data were aligned in time, thus eliminating issues associated with comparing SIF and GPP ensembles from different ranges of years. We found linear GPP-SIF relationships that were robust across both space and time. Further, the agreement between bottom-up and top-down scaling functions shows directly that upscaling using ecosystem-specific relationships in conjunction with SIF and knowledge of land cover distribution can yield robust landscape GPP estimates. The GPP_{SIF} proved to be a better regional-scale estimator compared to GPP_{MOD} despite employing a simple gridding and interpolation routine. Our results indicate that a single cropland-scaling function may be inappropriate, and at a minimum, different relationships for C_3 and C_4 crops should be derived. This is of particular significance in heavily cropped regions where one or more crops may dominate, e.g., intense corn-soybean versus rice production, suggesting that an average global cropland function may be unsuitable. Further studies directed toward determining the spread of GPP-SIF relationships in different natural ecosystems based on observational constraints will support the establishment and potential simplification of classification schemes for operational GPP estimation.

Acknowledgments
The authors would like to acknowledge funding support provided by the United States Department of Agriculture (USDA-NIFA2013-67019-21364) and the Minnesota Corn Research and Promotion Council (4101-15SP). Funding for this AmeriFlux core site was provided by the U.S. Department of Energy's Office of Science. We are grateful to the University of Minnesota Supercomputing Institute for partial support of this work. J.D.W. acknowledges U.S. Department of Energy support for the University of Missouri (subcontract 4000150689). Corn GPP data are available from AmeriFlux (http://ameriflux.lbl.gov/), and tall tower data are archived at http://www.biometeorology.umn.edu/. The solar-induced fluorescence data (v. B7101r) were produced by the OCO-2 project at the Jet Propulsion Laboratory, California Institute of Technology, and obtained from the OCO-2 data archive maintained at the NASA Goddard Earth Science Data and Information Services Center. The MODIS FPAR/LAI (MCD15A2 v5), GPP (MYD17A2H v6), and EVI/NDVI (MYD13Q1 v5) were obtained from the Land Processes DAAC. The authors declare no conflict of interest.

References

Anav, A., et al. (2015), Spatiotemporal patterns of terrestrial gross primary production: A review, *Rev. Geophys.*, *53*, 785–818, doi:10.1002/2015RG000483.

Baker, J. M., and T. J. Griffis (2005), Examining strategies to improve the carbon balance of corn/soybean agriculture using eddy covariance and mass balance techniques, *Agric. For. Meteorol.*, *128*(3-4), 163–177, doi:10.1016/j.agrformet.2004.11.005.

Baker, N. R. (2008), Chlorophyll fluorescence: A probe of photosynthesis in vivo, *Annu. Rev. Plant Biol.*, *59*, 89–113, doi:10.1146/annurev.arplant.59.032607.092759.

Beer, C., et al. (2010), Terrestrial gross carbon dioxide uptake: Global distribution and covariation with climate, *Science*, *329*(5993), 834–838, doi:10.1126/science.1184984.

Damm, A., L. Guanter, E. Paul-Limoges, C. van der Tol, A. Hueni, N. Buchmann, W. Eugster, C. Ammann, and M. E. Schaepman (2015), Far-red Sun-induced chlorophyll fluorescence shows ecosystem-specific relationships to gross primary production: An assessment based on observational and modeling approaches, *Remote Sens. Environ.*, *166*, 91–105, doi:10.1016/j.rse.2015.06.004.

Davis, K. J., P. S. Bakwin, C. Yi, B. W. Berger, C. Zhao, R. M. Teclaw, and J. G. Isebrands (2003), The annual cycles of CO_2 and H_2O exchange over a northern mixed forest as observed from a very tall tower, *Global Change Biol.*, *9*, 1278–1293, doi:10.1046/j.1365-2486.2003.00672.x.

Duveiller, G., and A. Cescatti (2016), Spatially downscaling Sun-induced chlorophyll fluorescence leads to an improved temporal correlation with gross primary productivity, *Remote Sens. Environ.*, *182*, 72–89, doi:10.1016/j.rse.2016.04.027.

Frankenberg, C., A. Butz, and G. C. Toon (2011a), Disentangling chlorophyll fluorescence from atmospheric scattering effects in O_2 A-band spectra of reflected sun-light, *Geophys. Res. Lett.*, *38*, L03801, doi:10.1029/2010GL045896.

Frankenberg, C., et al. (2011b), New global observations of the terrestrial carbon cycle from GOSAT: Patterns of plant fluorescence with gross primary productivity, *Geophys. Res. Lett.*, *38*, L17706, doi:10.1029/2011GL048738.

Frankenberg, C., C. O'Dell, J. Berry, L. Guanter, J. Joiner, P. Köhler, R. Pollock, and T. E. Taylor (2014), Prospects for chlorophyll fluorescence remote sensing from the Orbiting Carbon Observatory-2, *Remote Sens. Environ.*, *147*, 1–12, doi:10.1016/j.rse.2014.02.007.

Friedlingstein, P. (2015), Carbon cycle feedbacks and future climate change, *Philos. Trans. R. Soc. A*, *373*(2054), 20140421, doi:10.1098/rsta.2014.0421.

Gilmanov, T. G., et al. (2010), Productivity, respiration, and right-response parameters of world grassland and agroecosystems derived from flux-tower measurements, *Rangel. Ecol. Manage.*, *63*, 16–39, doi:10.2111/REM-D-09-00072.1.

Griffis, T. J., T. A. Black, K. Morgenstern, A. G. Barr, Z. Nesic, G. B. Drewitt, D. Gaumont-Guay, and J. H. McCaughey (2003), Ecophysiological controls on the carbon balances of three southern boreal forests, *Agric. For. Meteorol.*, *117*(1-2), 53–71, doi:10.1016/S0168-1923(03)00023-6.

Griffis, T. J., X. Lee, J. M. Baker, S. D. Sargent, and J. Y. King (2005), Feasibility of quantifying ecosystem-atmosphere $C^{18}O^{16}O$ exchange using laser spectroscopy and the flux-gradient method, *Agric. For. Meteorol.*, *135*(1-4), 44–60, doi:10.1016/j.agrformet.2005.10.002.

Griffis, T. J., J. Zhang, J. M. Baker, N. Kljun, and K. Billmark (2007), Determining carbon isotope signatures from micrometeorological measurements: Implications for studying biosphere-atmosphere exchange processes, *Boundary Layer Meteorol.*, *123*(2), 295–316, doi:10.1007/s10546-006-9143-8.

Griffis, T. J., S. D. Sargent, J. M. Baker, X. Lee, B. D. Tanner, J. Greene, E. Swiatek, and K. Billmark (2008), Direct measurement of biosphere-atmosphere isotopic CO_2 exchange using the eddy covariance technique, *J. Geophys. Res.*, *113*, D08304, doi:10.1029/2007JD009297.

Griffis, T. J., J. M. Baker, S. D. Sargent, M. Erickson, J. Corcoran, M. Chen, and K. Billmark (2010), Influence of C_4 vegetation on $^{13}CO_2$ discrimination and isoforcing in the upper Midwest, United States, *Global Biogeochem. Cycles*, *24*, GB4006, doi:10.1029/2009GB003768.

Guan, K., J. A. Berry, Y. Zhang, J. Joiner, L. Guanter, G. Badgley, and D. B. Lobell (2015), Improving the monitoring of crop productivity using spaceborne solar-induced fluorescence, *Global Change Biol.*, *22*, 716–726, doi:10.1111/gcb.13136.

Guanter, L., C. Frankenberg, A. Dudhia, P. E. Lewis, J. Gomez-Dans, A. Kuze, H. Suto, and R. G. Grainger (2012), Retrieval and global assessment of terrestrial chlorophyll fluorescence from GOSAT space measurements, *Remote Sens. Environ.*, *121*, 236–251, doi:10.1016/j.rse.2012.02.006.

Guanter, L., et al. (2014), Global and time-resolved monitoring of crop photosynthesis with chlorophyll fluorescence, *Proc. Natl. Acad. Sci. U.S.A.*, *111*(14), E1327–E1333, doi:10.1073/pnas.1320008111.

Huete, A., K. Didan, T. Miura, E. P. Rodriguez, X. Gao, and L. G. Ferreira (2002), Overview of the radiometric and biophysical performance of the MODIS vegetation indices, *Remote Sens. Environ.*, *83*(1-2), 195–213, doi:10.1016/S0034-4257(02)00096-2.

Joiner, J., Y. Yoshida, A. P. Vasilkov, Y. Yoshida, L. A. Corp, and E. M. Middleton (2011), First observations of global and seasonal terrestrial chlorophyll fluorescence from space, *Biogeosciences*, *8*(3), 637–651, doi:10.5194/bg-8-637-2011.

Joiner, J., L. Guanter, R. Lindstrot, M. Voigt, A. P. Vasilkov, E. M. Middleton, K. F. Huemmrich, Y. Yoshida, and C. Frankenberg (2013), Global monitoring of terrestrial chlorophyll fluorescence from moderate spectral resolution near-infrared satellite measurements: Methodology, simulations, and application to GOME-2, *Atmos. Meas. Tech. Discuss.*, *6*(2), 3883–3930, doi:10.5194/amtd-6-3883-2013.

Joiner, J., et al. (2014), The seasonal cycle of satellite chlorophyll fluorescence observations and its relationship to vegetation phenology and ecosystem atmosphere carbon exchange, *Remote Sens. Environ.*, *152*, 375–391, doi:10.1016/j.rse.2014.06.022.

Jung, M., et al. (2011), Global patterns of land-atmosphere fluxes of carbon dioxide, latent heat, and sensible heat derived from eddy covariance, satellite, and meteorological observations, *J. Geophys. Res.*, *116*, G00J07, doi:10.1029/2010JG001566.

Kljun, N., P. Calanca, M. W. Rotach, and H. P. Schmid (2004), A simple parameterisation for flux footprint predictions, *Boundary Layer Meteorol.*, *112*(3), 503–523, doi:10.1023/B:BOUN.0000030653.71031.96.

Liu, L., L. Guan, and X. Liu (2017), Directly estimating diurnal changes in GPP for C_3 and C_4 crops using far-red Sun-induced chlorophyll fluorescence, *Agric. For. Meteorol.*, *232*, 1–9, doi:10.1016/j.agrformet.2016.06.014.

Moffat, A. M., et al. (2007), Comprehensive comparison of gap-filling techniques for eddy covariance net carbon fluxes, *Agric. For. Meteorol.*, *147*(3-4), 209–232, doi:10.1016/j.agrformet.2007.08.011.

Parazoo, N. C., K. Bowman, J. B. Fisher, C. Frankenberg, D. B. A. Jones, A. Cescatti, Ó. Pérez-Priego, G. Wohlfahrt, and L. Montagnani (2014), Terrestrial gross primary production inferred from satellite fluorescence and vegetation models, *Global Change Biol.*, *20*(10), 3103–3121, doi:10.1111/gcb.12652.

Porcar-Castell, A., E. Tyystjärvi, J. Atherton, C. Van Der Tol, J. Flexas, E. E. Pfündel, J. Moreno, C. Frankenberg, and J. A. Berry (2014), Linking chlorophyll a fluorescence to photosynthesis for remote sensing applications: Mechanisms and challenges, *J. Exp. Bot.*, *65*(15), 4065–4095, doi:10.1093/jxb/eru191.

Reichstein, M., et al. (2005), On the separation of net ecosystem exchange into assimilation and ecosystem respiration: Review and improved algorithm, *Global Change Biol.*, *11*(9), 1424–1439, doi:10.1111/j.1365-2486.2005.001002.x.

Rossini, M., et al. (2015), Red and far red sun-induced cholorophyll fluorescence as a measure of plant photosynthesis, *Geophys. Res. Lett.*, *42*, 1632–1639, doi:10.1002/2014GL062943.

Ruimy, A., P. G. Jarvis, D. D. Baldocchi, and B. Saugier (1995), CO_2 fluxes over plant canopies and solar radiation: A review, *Adv. Ecol. Res.*, *26*, 1762–1776.

Suyker, A. E., and S. B. Verma (2012), Gross primary production and ecosystem respiration of irrigated and rainfed maize-soybean cropping systems over 8 years, *Agric. For. Meteorol.*, *165*, 12–24, doi:10.1016/j.agrformet.2012.05.021.

Yang, X., J. Tang, J. F. Mustard, J.-E. Lee, M. Rossini, J. Joiner, J. W. Munger, A. Kornfeld, and A. D. Richardson (2015), Solar-induced chlorophyll fluorescence correlates with canopy photosynthesis on diurnal and seasonal scales in a temperate deciduous forest, *Geophys. Res. Lett.*, *42*, 2977–2987, doi:10.1002/2015GL063201.

Yi, C., K. J. Davis, P. S. Bakwin, B. W. Berger, and L. C. Marr (2000), Influence of advection on measurements of the net ecosystem-atmosphere exchange of CO_2 from a very tall tower, *J. Geophys. Res.*, *105*, 9991–9999, doi:10.1029/2000JD900080.

Zhang, X., X. Lee, T. J. Griffis, J. M. Baker, and W. Xiao (2014), Estimating regional greenhouse gas fluxes: An uncertainty analysis of planetary boundary layer techniques and bottom-up inventories, *Atmos. Chem. Phys.*, *14*(19), 10,705–10,719, doi:10.5194/acp-14-10705-2014.

Zhang, Y., L. Guanter, J. A. Berry, J. Joiner, C. van der Tol, A. Huete, A. Gitelson, M. Voigt, and P. Kohler (2014), Estimation of vegetation photosynthetic capacity from space-based measurements of chlorophyll fluorescence for terrestrial biosphere models, *Global Change Biol.*, *20*(12), 3727–3742, doi:10.1111/gcb.12664.

Zhao, M., F. A. Heinsch, R. R. Nemani, and S. W. Running (2005), Improvements of the MODIS terrestrial gross and net primary production global data set, *Remote Sens. Environ.*, *95*(2), 164–176, doi:10.1016/j.rse.2004.12.011.